Effects of Induced Astigmatism on Spectral Domain-OCT Angiography Quantitative Metrics

JESSE J. JUNG, YU QIANG SOH, PATRICIA SHA, SOPHIA YU, MARY K. DURBIN, AND QUAN V. HOANG

• PURPOSE: To analyze the effect of induced astigmatism on en-face spectral-domain optical coherence tomography angiography quantitative metrics.
• DESIGN: Prospective crossover study.
• METHODS: Normal eyes without astigmatism and with 0.75, 1.75, and 2.75 diopters (D) of with-the-rule (WTR) astigmatism were imaged using a 3 × 3-mm scan pattern SD-OCTA CIRRUS 5000 HD-OCT with AngioPlex (Carl Zeiss Meditec, Dublin, CA, USA). Quantitative parameters, including foveal avascular zone metrics, parafoveal vessel length density (VD), and perfusion density (PD) were corrected for magnification secondary to axial length and analyzed. Univariate linear regressions were performed within each eye to correlate quantitative metrics to the level of an induced astigmatic cylinder.
• RESULTS: Fifteen eyes from 15 patients were imaged. Every 1-D increase in induced WTR astigmatism was associated with a statistically significant decrease in VD and PD within all Early Treatment Diabetic Retinopathy Study inner ring quadrants; however, especially more so nasally (VD: 0.63; $P < .001$; PD: 0.0089; $P = .001$). For every 1-D increase in induced astigmatism, the resulting decrease in the inner ring superior quadrant was 12% greater for VD and 16% greater for PD versus that in the inferior quadrant. The resulting decrease in the inner ring nasal quadrant was 40% greater for VD and 48% greater for PD versus that in the temporal quadrant.
• CONCLUSIONS: Increasing levels of induced WTR astigmatism correlated with globally diminishing VD and PD, was more symmetrical for vertical than horizontal quadrants, and was most pronounced nasally. This may be due to a high prevalence of horizontally oriented vessels nasally and the horizontal optical defocus induced by WTR astigmatism. (Am J Ophthalmol 2020;219: 49–58. © 2020 Elsevier Inc. All rights reserved.)

AJO.com Supplemental Material available at AJO.com.

Accepted for publication Jul 3, 2020.

From the East Bay Retina Consultants, Inc., Oakland, California, USA (J.J.J.); and Department of Ophthalmology, Universtiy of California, San Francisco, San Francisco, California, USA (J.J.J.); Singapore Eye Research Institute, Singapore National Eye Centre, Duke-NUS Medical School, Singapore, Singapore (Y.Q.S., Q.V.H.); Carl Zeiss Meditec, Inc., Dublin, California (P.S., S.Y., M.K.D.); Silicon Valley Eyecare Optometry, Santa Clara, California, USA (P.S.); and Department of Ophthalmology, Edward S. Harkness Eye Institute, Columbia College of Physicians and Surgeons, New York, New York USA (Q.V.H.).

Inquiries to Jesse J. Jung, East Bay Retina Consultants, Inc., 3300 Telegraph Ave, Oakland, CA 94609; e-mail: jung.jesse@gmail.com

OPTICAL COHERENCE TOMOGRAPHY ANGIOGraphy (OCTA) allows for noninvasive evaluation of retinal vascular architecture and flow patterns based on signal decorrelation characteristics across a set of successively acquired, high-resolution, cross-sectional retinal images.[1] Major advantages of OCTA over traditional fundus fluorescein angiography include rapid image acquisition,[2] depth-resolved image segmentation[1] (in particular, the ability to clearly image the deep capillary networks),[3] as well as the avoidance of discomfort due to intravenous exogenous fluorescein dye injection and associated risk of rare life-threatening allergic reactions.[4,5] Over the past decade, OCTA has been used for the diagnosis and monitoring of a wide range of retinal pathologies, such as retinal artery[6] or vein occlusions,[7–11] choroidal neovascularization,[12–14] retinal angiomatous proliferations,[15,16] polypoidal choroidal vasculopathy,[1,17,18] inflammatory conditions (eg, idiopathic multifocal choroiditis),[19,20] and diabetic retinopathy.[21–25]

However, OCTA is also known to be associated with a spectrum of image acquisition and processing artifacts that may negatively affect its reproducibility and reliability.[1,26,27] For example, image distortion arising from patient movement during OCTA acquisiton may result in a lower than expected vascular density.[26] Low-signal strength can affect the quality and reliability of quantitative metrics.[28] Defocus,[29] uncorrected axial length,[30] or media opacities in the vitreous and crystalline lens may result in the false appearance of a global vascular dropout.[31,32] Decentration, refraction shift, and tilt are also known to contribute toward poor image quality and result in non-reproducible readings across sequential imaging sessions.[33] Nonetheless, most of these artifacts, including decentration, refraction shift, tilt, and those classified as severe artifacts (e.g., shadow and defocus), can be corrected or mitigated by proper technician training and patient coaching.[26]

Refractive status such as axial myopia has been shown to be associated with changes in OCTA metrics, such as reduced vessel density and an enlarged foveal avascular zone (FAZ), possibly due to underlying anatomical alterations in keeping with pathological myopia, which may over time, progress to myopic maculopathy.[30,34–39] In addition, uncorrected spherical refractive defocus also affects OCTA image quality and can lead to an erroneous underestimation of vessel and perfusion density.[29] However, the exact correlation between the severity of astigmatic defocus and its effect on OCTA

0002-9394/$36.00
https://doi.org/10.1016/j.ajo.2020.07.005

quantitative metrics has not been elucidated. In contrast to spherical defocus, which results in a uniform optic blur, cylindrical defocus induces a varying gradient of optical blur across different meridians within the 3 × 3-mm OCTA scan area. Accordingly, we hypothesized that the presence of cylindrical defocus could result in an apparent decrease in vessel density on OCTA, albeit to a varying degree across the vertical and horizontal quadrants.

METHODS

THIS PROSPECTIVE, CROSSOVER, SINGLE-CENTER CLINICAL practice cohort study received prospective approval from the Salus Institutional Review Board (Austin, Texas, USA). This study complied with the Health Insurance Portability and Accountability Act of 1996 and followed the tenets of the Declaration of Helsinki. All subjects signed a written informed consent before participating in the study.

• **PARTICIPANTS:** Healthy eyes without significant astigmatism or intraocular pathologies were eligible for this study. Each eligible eye underwent non-mydriatic, autorefraction (Visuref 100, Carl Zeiss Meditec, Dublin, California, USA) to measure the amount of spherical and astigmatic correction. In addition, optical biometry, including axial length measurements, were obtained with the IOL Master 700 (Carl Zeiss Meditec, Dublin, CA, USA). Although there were no restrictions on spherical refractive errors, eyes were excluded if total astigmatism exceeded 0.25 diopters (D).

• **OCTA IMAGING:** Each eye underwent spectral-domain OCTA (SD-OCTA) with the CIRRUS 5000 Angioplex (Carl Zeiss Meditec, Dublin, CA, USA). SD-OCTA scanning was performed over a 3 × 3-mm region centered at the FAZ. All eyes were centered on the fovea, and high-quality SD-OCTA scans were obtained. Images were accepted only if they exhibited a signal strength of ≥8 (maximum signal strength for the AngioPlex software is 10), had correct segmentation, uniform illumination without areas of darkness, foveal centration, and minimal artifacts or saccades (identified as horizontal misalignment of vessel segments on en-face images). All images were obtained using the default commercial automated segmentation boundaries, and standard tracking software was used to minimize motion artifacts. Each en-face SD-OCTA image was generated using the optical microangiography (OMAG, Carl Zeiss Meditec, Dublin, CA, USA) algorithm at a resolution of 1,024 × 1,024 pixels, using 245 A-scans acquired at 245 B-scan positions. Each eye underwent SD-OCTA imaging at its baseline refractive error without astigmatism, followed by repeated imaging in the presence of with-the-rule (WTR) astigmatism induced via toric contact lenses of increasing power (+0.75, +1.75, and +2.75 D) in a randomized order to ensure the effect was not due to increased chair time or fatigue.

• **QUANTITATIVE MEASUREMENTS:** Regional analysis was performed following segmentation of the superficial retinal layer (SRL) in each SD-OCTA image based on the Early Treatment of Diabetic Retinopathy Study (ETDRS) parafoveal inner ring and central subfield. The ETDRS central subfield was defined as a central circle that measured 1,000 μm in diameter, centered at the fovea. The ETDRS inner ring was defined as a concentric ring with an inner diameter of 1,000 μm and an outer diameter of 3,000 μm centered at the fovea. The inner ring was further divided into 4 equal quadrants (superior, inferior, nasal, temporal) for subregion analysis. The ETDRS full ring was defined as the combined area represented by both the inner ring and central subfield. Each en-face SD-OCTA image was digitally analyzed with the Zeiss AngioPlex algorithm (version 10.0; available via a research license but not available in all markets, Carl Zeiss Meditec, Dublin, CA, USA) to quantify FAZ characteristics, SRL vessel length density (VD), and SRL perfusion density (PD). FAZ characteristics included size, perimeter, and circularity. Circularity was defined as the measure of the shape of the FAZ relative to a circle, with a higher value corresponding to a more circular shape. VD was defined as the total length of perfused vasculature per unit area of the image (mm^{-1}). PD was defined as the total area covered by perfused vasculature per unit area (unitless).

Quantitative metrics were corrected for the magnification factor due to variation in axial length, as described by Sampson et al.[30] using the Littman and modified Bennett formulas for the Zeiss AngioPlex (default axial length 24.46 mm, Carl Zeiss Meditec): $D_t^2/D_m^2 = 0.001949 \times (AL - 1.82)^2$; where D_t is the true physical linear dimension of the fundus, D_m is the measured OCTA image diameter, 1.82 is a constant related to the distance between the corneal apex and the second principal plane, and AL is the axial length. In short, according to the Littman formula, D_t can be expressed as $D_t = p \times q \times D_m$, where p (camera magnification factor) × q (ocular magnification factor) is the overall image magnification. The factor q can be determined from the Bennett formula: $q = 0.01306 \times (AL - 1.82)$. The factor p can be calculated from the Bennett formula if the axial length at which $D_t = D_m$ is known (24.46 mm). When $D_t = D_m$, then $p = 1/q$, and therefore, $p = 1/[0.01306(23.82\text{-}1.82)] = 3.38$. Thus, the adjustment in magnification factor was corrected by $D_t^2/D_m^2 = 0.001949 \times (AL - 1.82)^2$.

• **STATISTICAL ANALYSIS:** All data were analyzed with the Stata 15.1 statistical package (StataCorp LP, College Station, TX, USA). Univariate linear regression was performed to investigate the correlation between OCTA quantitative metrics and the level of induced WTR astigmatism. We included fixed effects for each individual eye

TABLE 1. Demographics

Total number of eyes (n)	15
Age (years)	40.9 (±12.8)
Laterality (right eye)	7 (47%)
Gender (male)	7 (47%)
Lens Status (phakic)	15 (100%)
Axial Length (mm)	24.32 (±1.3, Range 22.72-27.10)
Spherical Equivalent Refraction (diopters)	-2.43 (±2.91, Range -8 to +2.25)
Signal Strength	9.7 (±0.6, Range 8 to 10)

mm = millimeter; n = number

to use variation within an individual eye to estimate the effect of astigmatism on the outcome variables. By using fixed effects for our linear regressions, we accounted for variation in axial length (along with variation with any other possible confounding variable for which we were unaware) between eyes. Therefore, we used within variation versus variation across eyes, which allowed us to focus only on the variability within a given eye. In addition, standard errors were clustered on the eye level to account for the correlation in errors within each eye. All continuous variables are presented as mean ± standard deviation, unless otherwise stated. $P < .05$ was considered statistically significant.

RESULTS

A TOTAL OF 15 PATIENTS (15 EYES) WHO MET THE INCLUSION criteria were recruited for this study (Table 1). Average age was 40.9 years old, with a nearly equal distribution of right eyes versus left eyes (47% right eyes), and men versus women (47% men). All eyes were phakic, with an average axial length of 24.32 ± 1.3 mm; range: 22.72-27.10 mm), average spherical equivalent refractive error of −2.43 ± 2.91 D: range: −8 to +2.25 D), and an average SD-OCTA signal strength of 9.7 ± 0.6; range: 8-10).

The effects of induced astigmatism on FAZ, VD, and PD measurements are summarized in Table 2. Induced astigmatism did not result in any significant changes to FAZ size ($P = 0.85$), perimeter ($P = .54$), or circularity ($P = .11$). Each 1-D increase in induced astigmatism was associated with a 0.46 mm^{-1} decrease in central ring VD ($P = .002$), a 0.54 mm^{-1} decrease in inner ring VD ($P < .001$), and a 0.53 mm^{-1} decrease in full ring VD ($P < .001$). Subregion analysis within the inner ring further indicated a 0.57 mm^{-1} decrease in the ETDRS inner superior field VD ($P < .001$), a 0.51 mm^{-1} decrease in the ETDRS inner inferior field VD ($P < .001$), a 0.63 mm^{-1} decrease in ETDRS inner nasal field VD ($P < .001$), and a 0.45 mm^{-1} decrease in the ETDRS inner temporal field VD ($P = .003$) for each 1-D increase in induced astigmatism. Figure 1 is a representative example of the VD measurements from the lower end of the spectrum; it shows minimal changes induced in a right eye with no induced WTR astigmatism (Figure 1, A), 0.75-D WTR astigmatism (Figure 1, B), 1.75-D WTR astigmatism (Figure 1, C), and 2.75-D WTR astigmatism (Figure 1, D). Figure 2 is a representative example of the upper end of the spectrum that shows greater changes induced in a left eye with increasing levels of WTR astigmatism: 0.00 D (Figure 2, A), 0.75 D (Figure 2, B), 1.75 D (Figure 2, C), and 2.75 D (Figure 2, D). Finally, Figure 3 is a representative example of the VD measurements from the middle of the spectrum, showing mid-range changes induced in horizontal inner subfields of a right eye with increasing levels of WTR astigmatism: 0.00 D (Figure 3, A), 0.75 D (Figure 3, B), 1.75 D (Figure 3, C), and 2.75 D (Figure 3, D). Each 1-D increase in induced astigmatism was associated with a 0.0080 decrease in central ring PD ($P = .004$), a 0.0072 decrease in inner ring PD ($P < .001$), and a 0.0073 decrease in full ring PD ($P < .001$). Subregion analysis within the inner ring further indicated a 0.0074 decrease in the ETDRS inner superior field PD ($P = .002$), a 0.0064 decrease in the ETDRS inner inferior field PD ($P < .001$), a 0.0089 decrease in the ETDRS inner nasal field PD ($P = .001$), and a 0.0061 decrease in the ETDRS inner temporal field PD ($P = .022$) for each 1-D increase in induced astigmatism. The effect of induced WTR astigmatism was more symmetric for vertical quadrants and asymmetric for horizontal quadrants. For both VD and PD, vertical changes were intermediate, whereas nasal changes were the greatest, and temporal changes were the smallest. Specifically, for vertical quadrants, the resulting decrease (in response to a 1-D increase in induced WTR astigmatism) in the superior quadrant was 12% greater in magnitude for VD and 16% greater for PD than those in the inferior quadrant. In contrast, for horizontal quadrants, the differences were much larger in magnitude. Specifically, the resulting decrease (in response to a 1-D increase in induced WTR astigmatism) in the nasal quadrant was 40% greater in VD and 48% greater in PD than those in the temporal quadrant.

DISCUSSION

IN THIS STUDY, WE EVALUATED THE EFFECT OF INDUCED WTR astigmatism on SD-OCTA quantitative metrics in healthy eyes with no intraocular pathologies. Each 1-D increase in induced WTR astigmatism resulted in a generalized decrease in both VD and PD across all subfields within the 3 × 3-mm scan area, but there was no significant effect on FAZ metrics. In the horizontal axis, VD and PD depression were greater in the nasal quadrants than the temporal quadrants. In the vertical axis, VD and PD depression were

TABLE 2. Univariate Analysis of Changes in Quantiative Metrics due to Induced With-the-Rule Astigmatism

Variable	Regression Coefficient[a]	*P*
Foveal Avascular Zone (FAZ), mean values		
Size (mm^2)	−0.0003	.85
Perimeter (mm)	0.0062	.54
Circularity	−0.0065	.11
Vessel Density (VD), mean values (mm^{-1})		
Central Ring	−0.46	**.002***
Inner Ring	−0.54	**<.001***
Full Ring	−0.53	**<.001***
ETDRS Inner Superior Field	−0.57	**<.001***
ETDRS Inner Inferior Field	−0.51	**<.001***
ETDRS Inner Nasal Field	−0.63	**<.001***
ETDRS Inner Temporal Field	−0.45	**.003***
Perfusion Density (PD), mean values (unitless)		
Central Ring	−0.0080	**.004***
Inner Ring	−0.0072	**<.001***
Full Ring	−0.0073	**<.001***
ETDRS Inner Superior Field	−0.0074	**.002***
ETDRS Inner Inferior Field	−0.0064	**<.001***
ETDRS Inner Nasal Field	−0.0089	**.001***
ETDRS Inner Temporal Field	−0.0061	**.022***

ETDRS = Early Treatment Diabetic Retinopathy Study; FAZ = Foveal Avascular Zone; mm = millimeters; PD = Perfusion Density (unitless measure–total area of perfused vasculature per unit area in a region of measurement); VD = Vessel Density (mm^{-1} – total length of perfused vasculature per unit area in a region of measurement).

Bold face and (*) indicates statistical significance set at $P < .05$.

[a]Linear regression coefficient for each variable, per 1 diopter increase in induced with-the-rule astigmatism.

greater in the superior quadrants than the inferior quadrants. Comparing horizontal and vertical axes, VD and PD depression occurred more symmetrically within the vertical quadrants than within the horizontal quadrants.

The findings of this study suggested that the presence of optical astigmatism resulted in an underestimation of VD and PD values based on SD-OCTA, which were in keeping with previous reports of a generalized reduction in measured VD and PD values following spherical defocus.[29] A study of a single patient by Tomlison et al[29] demonstrated that a spherical defocus of −3.0 D resulted in a 10.4% decrease in VD measured by the AngioVue OCTA (Optovue, Fremont, CA, USA), despite acceptable quality readouts for all images. The effect of incorrect focus limited the ability to visualize fine capillary vessels and caused an apparent thickening of the remaining vasculature.[29] Current OCTA software can correct for spherical refractions but not astigmatism. The clinical implication of this effect is likely to be relevant when considering the use of SD-OCTA for evaluation of retinal pathologies in eyes with significant cylindrical refractive errors, as may be seen in pathologies such as keratoconus and other corneal ectasias. In this study, we induced WTR astigmatism up to 2.75 D, but the average corneal astigmatism in keratoconus is 4.0 D.[40,41] The use of SD-OCTA in these keratoconic eyes without appropriate refractive correction for optical astigmatism might result in inaccurately depressed VD and PD values in select quadrants. In addition, even mild keratoconus can progress in 25% of cases,[41] leading to worsening cylindrical refractive errors over time, thus affecting the validity of OCTA cross comparisons during longitudinal follow-up. Although this effect may be more significant in eyes with corneal astigmatism >3.0 D, this effect is likely less in the general population because the average corneal astigmatism is approximatley 0.50-1.50 D.[42,43] However, caution should be noted when following quantitative OCTA metrics longitudinally because the average astigmatism may increase and change with age from WTR to against-the-rule (ATR) astigmatism.[43] In addition, patients who have undergone surgical procedures, such as cataract extraction surgery, pterygium stripping, and other refractive procedures, may experience a sudden and significant change in their cylindrical refractive errors, which precludes an accurate comparison of OCTA scans acquired preprocedure versus postprocedure.

In this study, the placement of toric contact lenses of increasing powers (0.75, 1.75, and 2.75 D) induced WTR astigmatism of increasing magnitude. WTR astigmatism

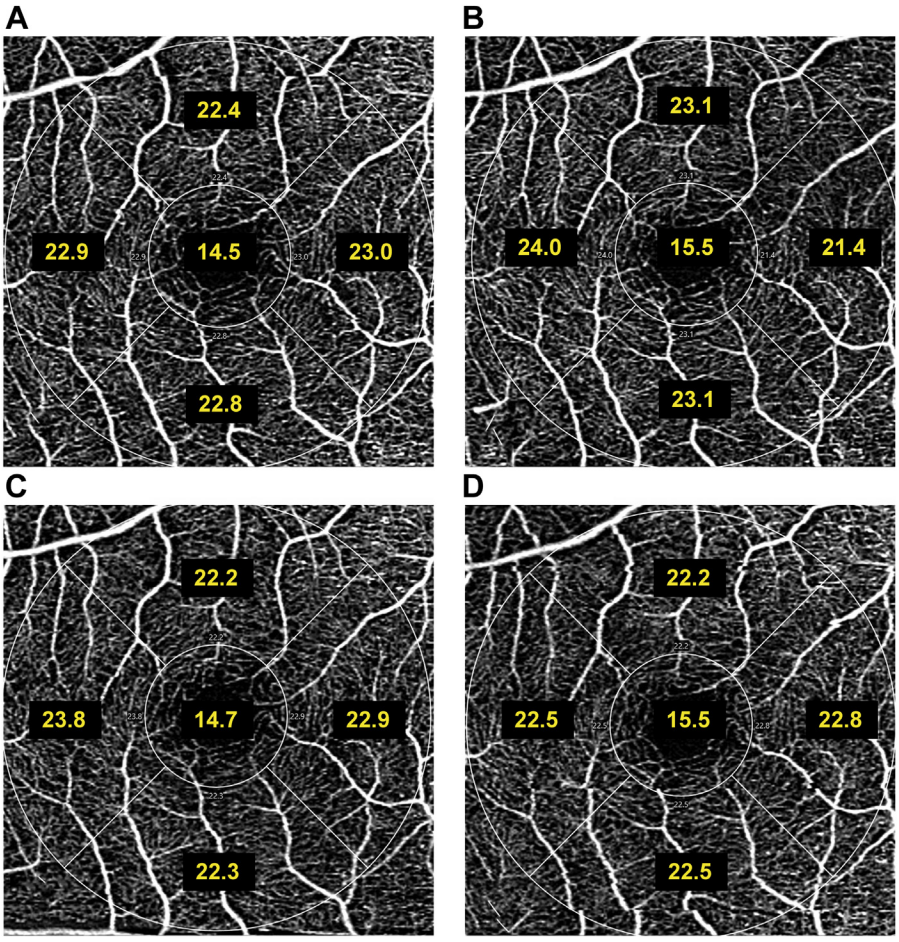

FIGURE 1. Example of an OCTA scan demonstrating minimal changes in vessel density in response to induced with-the-rule astigmatism. A right eye representative of the lower end of the spectrum, shows minimal changes in mean values of Early Treatment of Diabetic Retinopathy Study inner subfields (yellow text) induced by increasing levels of with-the-rule astigmatism (A: 0.00, B: 0.75, C: 1.75, D: 2.75 diopters). Note the minimal difference seen between the vertical and horizontal meridian absolute values (panels A versus D). This data was among those included in the linear regression analysis to assess the magnitude and significance of association between the level of induced astigmatism and OCTA metrics, the results of which are found in Table 2.

results in a horizontal optical defocus, which results in a greater obscuration of anatomical structures with a horizontal orientation than structures that are oriented vertically (Figures 1-3). Liu et al. previously evaluated the effect of WTR astigmatism on optical coherence tomography retinal nerve fiber layer (RNFL) measurements and noted that the eyes with higher levels of astigmatism had the appearance of a larger disc and rim area, thinner RNFL in the temporal quadrant, and farther temporally-positioned superotemporal and inferotemporal peak locations of RNFL thickness.[44] The effect of corneal astigmatism also resulted in an enhanced magnification effect that resulted in an optic disc that appeared more vertically oval and an inaccurate horizontal displacement of the scanning circle from the optic disc, which led to an artificially-decreased RNFL thickness measurement.[44] In addition, Hwang et al.[45] also induced WTR and ATR astigmatism with soft toric contact lenses and demonstrated that RNFL thicknesses of superior and inferior areas decreased after induction of a WTR astigmatism. These investigators also noted that RNFL thickness of nasal and temporal areas decreased after induction of an ATR astigmatism. By inducing significant degrees of astigmatism, this changed the scan distance from the optic disc and led to alterations in the RNFL thickness measurements.[45]

In the present study, we analyzed the effect of induced WTR astigmatism on quantitative measurements of the superficial retinal capillary vasculature. There may be an anatomic basis for our findings. On a general and macroscopic level, similar to retinal ganglion cells, retinal superficial capillary vasculature follow a predominantly horizontal orientation from nasal to the fovea, gradually transitioning to a near-vertical orientation temporal to

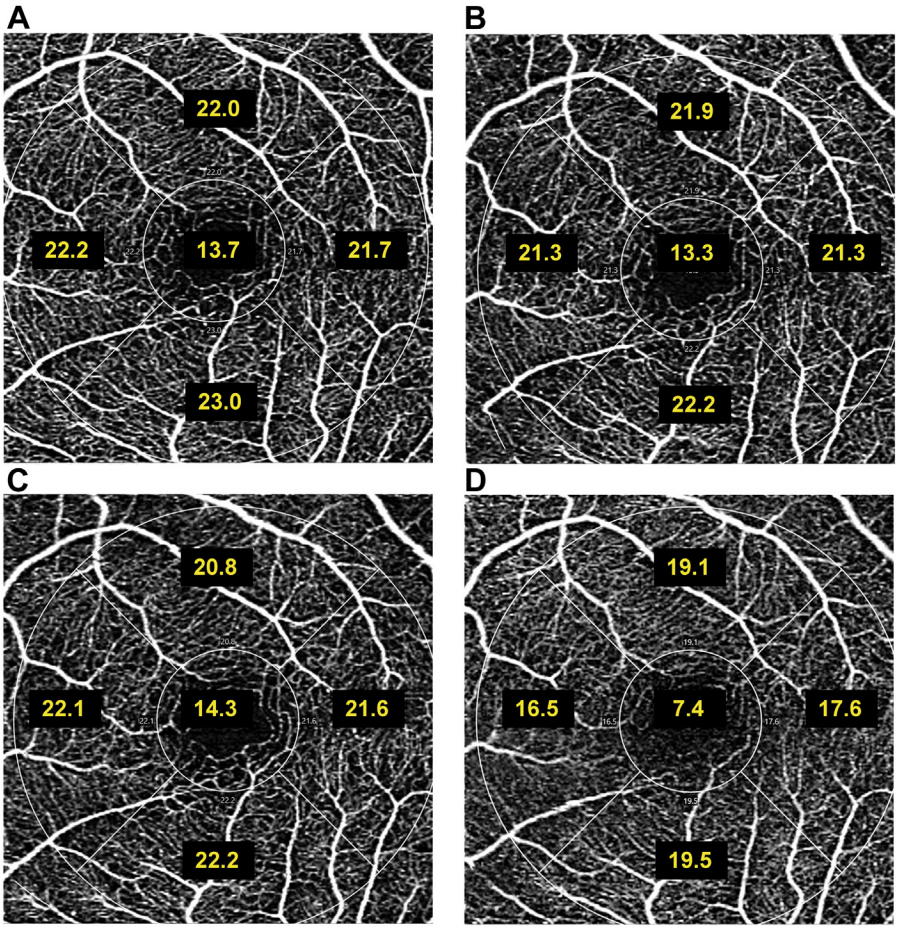

FIGURE 2. Example of an OCTA scan demonstrating extreme changes in vessel density in response to induced with-the-rule astigmatism. A left eye representative of the upper end of the spectrum, shows maximal changes in mean values of Early Treatment of Diabetic Retinopathy Study inner subfields (yellow text), induced by increasing levels of with-the-rule (WTR) astigmatism (A: 0.00, B: 0.75, C: 1.75, D: 2.75 diopters). Vessel density values were similar when comparing vertical and horizontal meridians, under conditions of no induced astigmatism (panel A). Under the influence of 2.75D of induced astigmatism (panel D), vessel density values were more affected in the horizontal meridian than the vertical meridian. This data was among those included in the linear regression analysis to assess the magnitude and significance of association between the level of induced astigmatism and OCTA metrics, the results of which are found in Table 2.

the fovea while following an intermediate orientation in the regions superior and inferior to the fovea.[46] However, on a microscopic level, it is apparent that horizontally-oriented vessels can be found and imaged within the SRL at all regions around the fovea, especially among finer vessels within the higher order branches of the capillary bed.[47] We found that induced WTR astigmatism resulted in selective obscuration of horizontally-oriented retinal capillary vasculature that was present in all ETDRS quadrants, thus leading to progressively and globally reduced quantitative metrics with increased diopters of astigmatism. The observation of a disparately larger effect of increased induced astigmatism on VD and PD reduction in the nasal quadrant could also be explained by the fact that the nasal quadrant naturally has, as explained previously, a higher density of horizontally-oriented SRL capillaries.

Current OCTA systems use an ocular lens to bring the retina into focus for a wide range of spherical refractive errors, but these do not correct for the meridional effects of astigmatism-induced magnification errors. The mathematical correction of spherical refraction-induced image magnification is based on the Littmann formula,[48] which was first described in 1982 and subsequently refined by Bennett et al. in 1994.[49] The Littman formula states that the true anatomical dimension of a retinal feature (t) is dependent on an interaction between the measured dimension (s), camera magnification factor (p), and ocular magnification factor (q).[44] In determining the effects of ametropia on the ocular magnification factor (q), any existing astigmatism is most commonly dealt with by collapsing the optical powers along the 2 principal axes into a single spherical equivalent term while ignoring the axis direction.

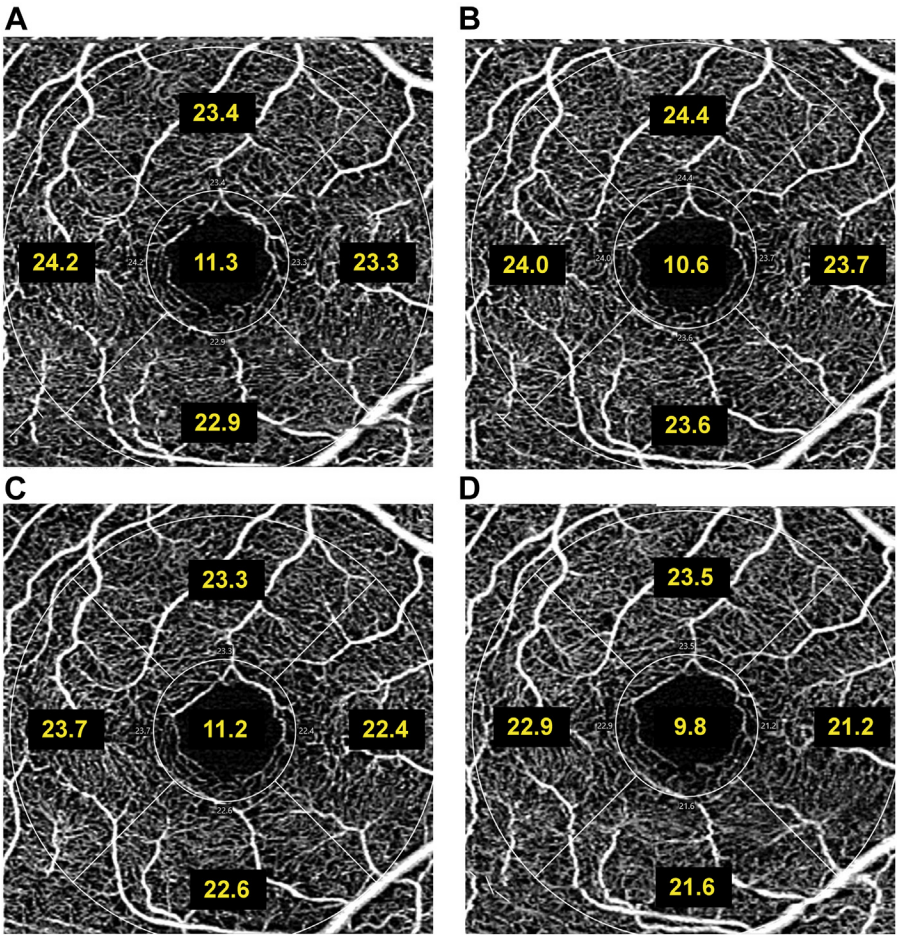

FIGURE 3. Example of an OCTA scan demonstrating mid-range changes in vessel density in response to induced with-the-rule astigmatism. A right eye representative of the middle of the spectrum, shows mid-range changes* (*mid-range values differed between horizontal and vertical meridians; for the purpose of this illustration, mid-range values refer to those observed within horizontal Early Treatment of Diabetic Retinopathy Study (ETDRS) inner subfields) in mean values of ETDRS inner subfields (yellow text), induced by increasing levels of with-the-rule astigmatism (A: 0.00, B: 0.75, C: 1.75, D: 2.75 diopters). Note the relatively larger changes (comparing panels A and D) in horizontal subfields (nasal and temporal) versus vertical subfields (superior and inferior). This data was among those included in the linear regression analysis to assess the magnitude and significance of association between the level of induced astigmatism and OCTA metrics, the results of which are found in Table 2.

Although this is a common practice, it nonetheless results in a masking of the actual meridional effects of astigmatism-induced magnification errors. This factor emerges as a key consideration, especially when making comparisons of dimension sizes between orthogonally-oriented anatomical features (e.g., SRL capillaries) in different anatomical quadrants.

This study provided important information about the ability to reliably analyze quantitative metrics in eyes with induced astigmatism. Despite the presence of statistically significant effects of increasing astigmatism on OCTA metrics, the amount of reduction in VD and PD was relatively small even up to an induced astigmatism of 2.75 D. As such, uncorrected astigmatism might have a limited effect on the overall reliability and reproducibility of OCTA metrics for most patients. However, such a measurement error might increase and effectively shift location as the cornea develops more ATR astigmatism with age. In addition, this effect would be expected to be exacerbated, and therefore, more clinically relevant especially in pathological corneal ectatic conditions (e.g., keratoconus), in which the average baseline corneal astigmatism is known to be >3.0 D, with a possibility of progression to a range of 10-15 D in extreme cases.[41,50]

Limitations of this study include the relatively small sample size and the use of only a single SD-OCTA system (the AngioPlex, Carl Zeiss Meditec, Inc., Dublin, CA, USA), and thus the results may not be reproducible across other commercial platforms. Even with a small sample size, this exploratory study achieved statistical significance across most of our regression analyses and appeared more than sufficient for analyzing the included outcome

variables. Furthermore, we included eyes with, on average, −2.43 D of myopia. However, the effect of this defocus was mitigated by adjusting the spherical focus on the SD-OCTA during image acquisition. The SD-OCTA used a telecentric lens that allowed for a standard field of view for all images acquired. The effect of magnification due to variability in axial lengths might also have affected the quantification of vessel density metrics. To confirm our statistical approaches were robust, we adjusted for axial length–induced magnification based on the findings of Sampson et al.[30] In addition, the effect of axial length on the parafoveal superficial retinal vessel density was relatively small (ranging: −3% to +2%) for a refractive error that ranged from −8.00 to +4.88 D and axial length from 21.27-28.85 mm.[30] In their study, the included eyes had a greater range in refractive error and axial length than what was noted in this present study (refractive range of −8.00 to +2.25 D and axial length 22.72-27.10 mm). This minimal loss of data (or gain of data) contained within the ETDRS parafoveal inner ring due to magnification issues was also fully accommodated statistically with the fixed effects used for the linear regression analysis. This allowed us to focus on the changes within the ETDRS inner subfields within a given eye across the 4 levels of induced astigmatism (0, +0.75, +1.75, and +2.75 D). Moreover, our subanalysis compared intra-eye changes in the vertical (superior and inferior) versus horizontal (nasal and temporal) subfields, and not inter-eye changes, which are at higher risk for this confounding effect. Finally, automated segmentation boundaries could have led to possible segmentation errors and affect the quantitative metrics analysis. We attempted to minimize the amount of artifact errors by studying healthy, normal eyes with high quality, correctly segmented and focused images, and strong signal strength.

CONCLUSIONS

IN CONCLUSION, OUR STUDY IS THE FIRST TO DEMONstrate the qualitative and quantitative effects of induced astigmatism on SD-OCTA SRL metrics. Measurements within the entire macula were affected by induced WTR astigmatism, with the largest effect found nasally. Astigmatic shifts were likely to confound both time-based and meridional cross comparisons of these measurements, especially in the presence of high astigmatic errors.

A) FUNDING/SUPPORT: THIS WORK WAS SUPPORTED IN PART BY AN UNRESTRICTED GRANT FROM RESEARCH TO PREVENT Blindness (RPB), United States, K08 Grant (QVH, 1 K08 EY023595, National Eye Institute, United States, NIH) and National Medical Research Council (NMRC), Singapore Clinician Scientist Award Grant (QVH, CSA-INVMay0011, Singapore). The sponsor or funding organization had no role in the design or conduct of this research.

b) Financial Disclosures: J.J.J. has been a consultant for Carl Zeiss Meditec, Inc., Alimera Sciences, Allergan, and Google. P.S., S.Y., M.K.D. are employed by Carl Zeiss Meditec, Inc. Q.V.H. has received research support from Johnson & Johnson. All other authors have reported that they have no relationships relevant to the contents of this paper to disclose.

c) Design of the study (J.J.J., P.S., Q.V.H.), Conduct of the study (J.J.J., P.S., S.Y.), Collection of the data (S.Y., P.S.), Management of the data (J.J.J., Y.Q.S., P.S., QVH), Analysis of the data (J.J.J., Y.Q.S., S.Y., P.S., M.K.D., Q.V.H.), Interpretation of the data (J.J.J., Y.Q.S., P.S., M.K.D., Q.V.H.), Preparation of the manuscript (J.J.J., Y.Q.S., Q.V.H.), Review of the manuscript (J.J.J., Y.Q.S, P.S., S.Y., M.K.D., Q.V.H.), and Approval of the manuscript (J.J.J., Y.Q.S., P.S., S.Y., M.K.D., Q.V.H.).

REFERENCES

1. Spaide RF, Fujimoto JG, Waheed NK, Sadda SR, Staurenghi G. Optical coherence tomography angiography. *Prog Retin Eye Res* 2018;64:1–55.
2. Migacz JV, Gorczynska I, Azimipour M, Jonnal R, Zawadzki RJ, Werner JS. Megahertz-rate optical coherence tomography angiography improves the contrast of the choriocapillaris and choroid in human retinal imaging. *Biomed Opt Express* 2019;10(1):50–65.
3. Spaide RF, Klancnik JM, Cooney MJ. Retinal vascular layers imaged by fluorescein angiography and optical coherence tomography angiography. *JAMA Ophthalmol* 2015;133(1):45–50.
4. Yannuzzi LA, Rohrer KT, Tindel LJ, et al. Fluorescein angiography complication survey. *Ophthalmology* 1986;93(5):611–617.
5. Karhunen U, Raitta C, Kala R. Adverse reactions to fluorescein angiography. *Acta Ophthalmol* 1986;64(3):282–286.
6. Jung JJ, Chen MH, Lee SS. Branch retinal artery occlusion imaged with spectral-domain optical coherence tomographic angiography. *JAMA Ophthalmol* 2016;134(4):e155041.
7. Kogo T, Muraoka Y, Iida Y, et al. Angiographic risk features of branch retinal vein occlusion onset as determined by optical coherence tomography angiography. *Invest Ophthalmol Vis Sci* 2020;61(2):8.
8. Ogasawara Y, Iwase T, Yamamoto K, Ra E, Terasaki H. Relationship between abnormalities of photoreceptor microstructures and microvascular structures determined by optical coherence tomography angiography in eyes with branch retinal vein occlusion. *Retina* 2020;40(2):350–358.
9. Sakimoto S, Kawasaki R, Nishida K. Retinal neovascularization–simulating retinal capillary reperfusion in branch retinal vein occlusion, imaged by wide-field optical coherence tomography angiography. *JAMA Ophthalmol* 2020;138(2):216–218.
10. Nagasato D, Tabuchi H, Masumoto H, et al. Automated detection of a nonperfusion area caused by retinal vein

occlusion in optical coherence tomography angiography images using deep learning. *PLoS One* 2019;14(11):e0223965.
11. Jung JJ, Chen MH, Shi Y, et al. Correlation of en face optical coherence tomography angiography averaging versus single-image quantitative measurements with retinal vein occlusion visual outcomes. *Retina* 2019;40:786–794.
12. Arrigo A, Romano F, Aragona E, et al. Optical coherence tomography angiography can categorize different subgroups of choroidal neovascularization secondary to age-related macular degeneration. *Retina* 2020; https://doi.org/10.1097/IAE.0000000000002775.
13. Hikichi T, Agarie M, Kubo N, Yamauchi M. Predictors of recurrent exudation in choroidal neovascularization in age-related macular degeneration during a treatment-free period. *Retina* 2020; https://doi.org/10.1097/IAE.0000000000002745.
14. Faatz H, Farecki M-L, Rothaus K, Gutfleisch M, Pauleikhoff D, Lommatzsch A. Changes in the OCT angiographic appearance of type 1 and type 2 CNV in exudative AMD during anti-VEGF treatment. *BMJ Open Ophthalmol* 2019;4(1):e000369.
15. Yeo JH, Chung H, Kim JT. Swept-source optical coherence tomography angiography according to the type of choroidal neovascularization. *J Clin Med* 2019;8(9):1272.
16. de Jong JH, Braaf B, Amarakoon S, et al. Treatment effects in retinal angiomatous proliferation imaged with OCT angiography. *Ophthalmologica* 2019;241(3):143–153.
17. Le Rouic J-F, Peronnet P, Barrucand A, et al. [Indications for fluorescein angiography and optical coherence tomography angiography (OCTA) in medical retina: Changes from 2015 and 2018]. *J Fr Ophtalmol* 2020;43(5):397–403.
18. Cheung CMG, Yanagi Y, Akiba M, et al. Improved detection and diagnosis of polypoidal choroidal vasculopathy using a combination of optical coherence tomography and optical coherence tomography angiography. *Retina* 2019;39(9):1655–1663.
19. Zahid S, Chen KC, Jung JJ, et al. Optical coherence tomography angiography of chorioretinal lesions due to idiopathic multifocal choroiditis. *Retina* 2017;37(8):1451–1463.
20. Dutheil C, Korobelnik J-F, Delyfer M-N, Rougier M-B. Optical coherence tomography angiography and choroidal neovascularization in multifocal choroiditis: a descriptive study. *Eur J Ophthalmol* 2018;28(5):614–621.
21. Sandhu HS, Elmogy M, El-Adawy N, et al. Automated diagnosis of diabetic retinopathy using clinical biomarkers, optical coherence tomography (OCT), and OCT angiography. *Am J Ophthalmol* 2020;216:201–206. https://doi.org/10.1016/j.ajo.2020.01.016.
22. Marques IP, Alves D, Santos T, et al. Characterization of disease progression in the initial stages of retinopathy in type 2 diabetes: a 2-year longitudinal study. *Invest Ophthalmol Vis Sci* 2020;61(3):20.
23. Forte R, Haulani H, Jürgens I. Quantitative and qualitative analysis of the three capillary plexuses and choriocapillaris in patients with type 1 and type 2 diabetes mellitus without clinical signs of diabetic retinopathy: a prospective pilot study. *Retina* 2020;40(2):333–344.
24. Choi EY, Park SE, Lee SC, et al. Association between clinical biomarkers and optical coherence tomography angiography parameters in type 2 diabetes mellitus. *Invest Ophthalmol Vis Sci* 2020;61(3):4.
25. Battista M, Borrelli E, Sacconi R, Bandello F, Querques G. Optical coherence tomography angiography in diabetes: a review. *Eur J Ophthalmol* 2020;30(3):411–416. https://doi.org/10.1177/1120672119899901.
26. Holmen IC, Konda MS, Pak JW, et al. Prevalence and severity of artifacts in optical coherence tomographic angiograms. *JAMA Ophthalmol* 2019;138(2):119–126. https://doi.org/10.1001/jamaophthalmol.2019.4971.
27. Spaide RF, Fujimoto JG, Waheed NK. Image artifacts in optical coherence tomography angiography. *Retina Phila Pa* 2015;35(11):2163–2180.
28. Lim HB, Kim YW, Kim JM, Jo YJ, Kim JY. The importance of signal strength in quantitative assessment of retinal vessel density using optical coherence tomography angiography. *Sci Rep* 2018;8(1):1–8.
29. Tomlinson A, Hasan B, Lujan BJ. Importance of focus in OCT angiography. *Ophthalmol Retina* 2018;2(7):748–749.
30. Sampson DM, Gong P, An D, et al. Axial length variation impacts on superficial retinal vessel density and foveal avascular zone area measurements using optical coherence tomography angiography. *Invest Ophthalmol Vis Sci* 2017;58(7):3065–3072.
31. Holló G. Influence of Posterior subcapsular cataract on structural OCT and OCT angiography vessel density measurements in the peripapillary retina. *J Glaucoma* 2019;28(4):e61–e63.
32. Yu S, Frueh BE, Steinmair D, et al. Cataract significantly influences quantitative measurements on swept-source optical coherence tomography angiography imaging. *PLoS One* 2018;13(10):e0204501.
33. De Pretto LR, Moult EM, Alibhai AY, et al. Controlling for artifacts in widefield optical coherence tomography angiography measurements of non-perfusion area. *Sci Rep* 2019;9(1):1–15.
34. Li Y, Miara H, Ouyang P, Jiang B. The comparison of regional RNFL and fundus vasculature by OCTA in Chinese myopia population. *J Ophthalmol* 2018;2018:3490962.
35. Leng Y, Tam EK, Falavarjani KG, Tsui I. Effect of age and myopia on retinal microvasculature. *Ophthalmic Surg Lasers Imaging Retina* 2018;49(12):925–931.
36. Gołębiewska J, Biała-Gosek K, Czeszyk A, Hautz W. Optical coherence tomography angiography of superficial retinal vessel density and foveal avascular zone in myopic children. *PLoS One* 2019;14(7):e0219785.
37. Saw S-M, Matsumura S, Hoang QV. Prevention and management of myopia and myopic pathology. *Invest Ophthalmol Vis Sci* 2019;60(2):488–499.
38. Ang M, Wong CW, Hoang QV, et al. Imaging in myopia: potential biomarkers, current challenges and future developments. *Br J Ophthalmol* 2019;103(6):855–862.
39. Hoang QV, Chua J, Ang M, Schmetterer L. Imaging in myopia. In: Ang M, Wong TY, eds. Updates on Myopia: A Clinical Perspective. Singapore: Springer; 2020:219–239.
40. Aslani F, Khorrami-Nejad M, Aghazadeh Amiri M, Hashemian H, Askarizadeh F, Khosravi B. Characteristics of posterior corneal astigmatism in different stages of keratoconus. *J Ophthalmic Vis Res* 2018;13(1):3–9.
41. Choi JA, Kim M-S. Progression of keratoconus by longitudinal assessment with corneal topography. *Invest Ophthalmol Vis Sci* 2012;53(2):927–935.

42. Pontikos N, Chua S, Foster PJ, Tuft SJ, Day AC, UK Biobank Eye and Vision Consortium. Frequency and distribution of corneal astigmatism and keratometry features in adult life: methodology and findings of the UK Biobank study. *PLoS One* 2019;14(9):e0218144.
43. Collier Wakefield O, Annoh R, Nanavaty MA. Relationship between age, corneal astigmatism, and ocular dimensions with reference to astigmatism in eyes undergoing routine cataract surgery. *Eye Lond Engl* 2016;30(4):562–569.
44. Liu L, Zou J, Huang H, Yang J, Chen S. The influence of corneal astigmatism on retinal nerve fiber layer thickness and optic nerve head parameter measurements by spectral-domain optical coherence tomography. *Diagn Pathol* 2012;7(1):55.
45. Hwang YH, Lee SM, Kim YY, Lee JY, Yoo C. Astigmatism and optical coherence tomography measurements. *Graefes Arch Clin Exp Ophthalmol* 2012;250(2):247–254.
46. Scoles D, Gray DC, Hunter JJ, et al. In-vivo imaging of retinal nerve fiber layer vasculature: imaging histology comparison. *BMC Ophthalmol* 2009;9:9.
47. Zhu Q, Xing X, Zhu M, et al. A new approach for the segmentation of three distinct retinal capillary plexuses using optical coherence tomography angiography. *Transl Vis Sci Technol* 2019;8(3):57.
48. Littmann H. [Determining the true size of an object on the fundus of the living eye]. *Klin Monatsbl Augenheilkd* 1988;192(1):66–67.
49. Bennett AG, Rudnicka AR, Edgar DF. Improvements on Littmann's method of determining the size of retinal features by fundus photography. *Graefes Arch Clin Exp Ophthalmol* 1994;232(6):361–367.
50. Savini G, Næser K, Schiano-Lomoriello D, Mularoni A. Influence of posterior corneal astigmatism on total corneal astigmatism in eyes with keratoconus. *Cornea* 2016;35(11):1427–1433.